


RESEARCH ARTICLE | AUGUST 16 2022

## Impact of a continuously extending wall on laminar-turbulent transition in subsonic boundary layers

Ming Dong (董明) 



*Physics of Fluids* 34, 084109 (2022)

<https://doi.org/10.1063/5.0106736>



View  
Online



Export  
Citation

CrossMark

### Articles You May Be Interested In

Scattering of Mack modes by solid-porous junctions in hypersonic boundary layers

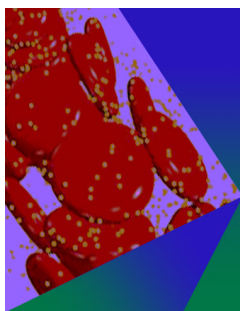
*Physics of Fluids* (August 2022)

Revisit of the oblique-breakdown regime in supersonic boundary layers and mechanism of the extra amplification of streak modes

*Physics of Fluids* (October 2022)

A structural subgrid-scale model for the collision-related statistics of inertial particles in large-eddy simulations of isotropic turbulent flows

*Physics of Fluids* (September 2020)



## Physics of Fluids

### Special Topic: Flow and Forensics

Submit Today!



# Impact of a continuously extending wall on laminar-turbulent transition in subsonic boundary layers

Cite as: Phys. Fluids **34**, 084109 (2022); doi: [10.1063/5.0106736](https://doi.org/10.1063/5.0106736)

Submitted: 29 June 2022 · Accepted: 28 July 2022 ·

Published Online: 16 August 2022




View Online



Export Citation



CrossMark

Ming Dong (董明)<sup>1,2,a)</sup> 

## AFFILIATIONS

<sup>1</sup>State Key Laboratory of Nonlinear Mechanics, Institute of Mechanics, Chinese Academy of Sciences, Beijing 100190, China

<sup>2</sup>Sino-Russian Mathematics Center, Peking University, Beijing 100871, China

<sup>a)</sup> Author to whom correspondence should be addressed: [dongming@imech.ac.cn](mailto:dongming@imech.ac.cn)

## ABSTRACT

Structural morphing is an efficient means to enable the design of aircrafts for diverse requirements, such as high endurance and high speed; however, there may be side effects on the aerodynamic performance, which needs to be considered before its implementation. In this paper, we particularly focus on the impact of a representative morphing structure, a continuously extending wall in the chordwise direction, on the laminar-turbulent transition in subsonic boundary layers. The large-Reynolds-number asymptotic approach is employed, and both the mean-flow distortion and the perturbation field are described by the triple-deck theory, which leads to a great reduction in the number of the controlling parameters and shows clearly their interaction mechanisms. Two relevant mechanisms, namely, the local receptivity and local scattering mechanisms, are considered, whose effects on the development of the boundary-layer instability modes, leading to a change in the transition onset eventually, are quantified systematically by solving numerically the high-dimensional linear equation system. The receptivity efficiency is greater near the lower-branch neutral frequency, while the scattering effect increases with the frequency monotonically. Both the receptivity and scattering calculations show good agreement with the linear predictions when the extending-wall speed is sufficiently low, but for a moderate extending speed, both the receptivity efficiency and the scattering efficiency increase superlinearly with the extending speed.

Published under an exclusive license by AIP Publishing. <https://doi.org/10.1063/5.0106736>

## I. INTRODUCTION

With the progressively increasing requirement of the aviation sector in the modern world, many new technologies and novel concepts are developed to improve the aircraft performance. In order to execute multiple tasks in a more efficient way, structural morphing is preferred in the aircraft designs, which, however, requires consideration of many fundamental problems relating to the aerodynamic performance of the flying vehicles. Laminar-turbulent transition in boundary-layer flows is an unavoidable problem in aerodynamic designs due to its direct relevance to surface friction, and it is of practical importance to study the morphing effect on transition before its implementation. There have been quite a few morphing strategies for subsonic and transonic flights, including planform alternations (chord, span, and sweep), out-of-plane transformations (twist, dihedral/gull, and spanwise bending), and airfoil adjustment (camber and thickness).<sup>1,2</sup> In this paper, we particularly focus on the effect of an extendable wall in the chordwise direction in subsonic boundary layers.

When the wall is extending, the boundary condition of the fluids at the extending point becomes discontinuous, which leads to a rapid mean-flow distortion in a localized region. Such a distortion could either interact with the freestream perturbations, exciting the boundary-layer instability modes due to the receptivity regime, or interact with the oncoming boundary-layer instability modes, leading to a rapid distortion of the latter due to the local scattering regime. The two regimes affect the accumulation of the instability modes, which eventually leads to a movement of the transition onset. In order to predict this movement, the two aforementioned regimes need to be described quantitatively.

In order to describe the excitation of the Tollmien-Schlichting (TS) waves due to the interaction of freestream acoustic waves and roughness, Ruban<sup>3</sup> and Goldstein<sup>4</sup> developed the first local receptivity theory, separately. Because both the roughness-induced mean-flow distortion and TS instability are concentrated in a near-wall thin layer and have the same length scales in the streamwise direction, their behaviors and interaction could be described by the same formalism,

the triple-deck formalism. The receptivity efficiency was quantified by use of the residual theorem due to the appearance of a discrete pole in the spectrum solution of the excited perturbation. This theoretical framework was subsequently extended to the vorticity–roughness interaction,<sup>5,6</sup> the entropy–roughness interaction,<sup>7</sup> and the vorticity–acoustic interaction.<sup>8</sup> Such a local receptivity theory also applies for transonic configurations,<sup>9</sup> and even the receptivity of the three-dimensional Mack first modes with large oblique angles in supersonic boundary layers.<sup>10</sup> However, for the Mack second or higher-order modes and the quasi-two-dimensional first modes, the local receptivity is described by a different asymptotic theory.<sup>11</sup> This paper considers the morphing-wall effect in subsonic boundary layers in which the instability is of the viscous TS nature, and so its local receptivity due to the interaction of the morphing wall and freestream acoustic waves can be described by the same framework as in the Ruban–Goldstein theory.<sup>3,4</sup> It is, however, interesting to note that if the extending speed of the morphing wall is comparable with the characteristic velocity in the lower deck, i.e., the nonlinearity comes into the leading order, then the excited TS instability downstream of the extending point shows a different dispersion relation from the oncoming TS instability. This can be interpreted as the Doppler effect in a moving frame.

The local scattering of the oncoming TS waves by localized roughness in subsonic boundary layers was theoretically formulated by Wu and Dong,<sup>12</sup> in which a transmission coefficient was introduced to quantify the amplitude change in the perturbations due to the scattering effect. Again, the triple-deck formalism was employed, which helps to reveal the physical mechanism for the TS–roughness interaction. Because in the large-Reynolds-number approximation, the TS waves upstream and downstream of the roughness have the same shape profiles, although with different amplitudes, a generalized eigenvalue problem, with the transmission coefficient appearing as the eigenvalue, was formulated. This transmission coefficient can be integrated in the traditional e-N transition prediction method to take into account the roughness impact. Such a framework was latter applied to describe the TS-step and TS-step-suction interactions<sup>13,14</sup> and the scattering problem in transonic configurations.<sup>15</sup> Note that the scattering mechanism of the inviscid Mack modes in a supersonic or hypersonic boundary layer is completely different, as revealed by Refs. 16 and 17. At a finite Reynolds number, the scattering efficiency for both the low- and high-speed regimes can be alternatively obtained by the harmonic linearized Navier–Stokes approach,<sup>18,19</sup> direct numerical simulations,<sup>20</sup> and experiments.<sup>21,22</sup> However, the asymptotic description is more desirable for revealing the underlining mechanism. For the morphing wall in subsonic boundary layers, the majority formulation of Ref. 12 can be applied; however, the morphing wall induces a Doppler effect on the TS instability, rendering a discrepancy of the perturbation profile in the downstream limit from the oncoming one. Thus, the generalized eigenvalue problem is not recovered, and a modification of the formula system is required.

The rest part of this paper is structured as follows. The physical model and the governing equations are introduced in Secs. II A and II B, respectively, followed by the triple-deck descriptions of the mean flow in Sec. II C and the perturbations Sec. II D. The inflow perturbations for the receptivity and local scattering calculations are introduced in Secs. II E and II F, respectively, and the receptivity and transmission coefficients for quantifying the two regimes are introduced in Sec. II G.

The numerical results are shown in Sec. III, and finally, we present the concluding remarks in Sec. IV.

## II. PHYSICAL MODEL AND MATHEMATICAL DESCRIPTIONS

### A. Physical model

In order to show the impact of the morphing effect on the instability evolution in a boundary layer over a wing, we choose a simplified model, namely, a flat plate that is extending continuously from a location with a distance  $L$  to its leading edge; see Fig. 1. The plate is divided into two subplates, and the second one is moving tangentially with a constant speed  $u_s^*$ . For simplicity, we assume the plate at the extending point to be smooth with no steps or gaps, and the wall is assumed to be isothermal. The moving plate is arranged in a uniform subsonic stream with zero angle of attack. Two related mechanisms are considered (see the sketch in Fig. 1): (1) when an incident plane sound wave is introduced in the free stream, its interaction with the rapidly distorted mean flow around the extending point leads to the receptivity of the TS waves; (2) when an oncoming TS wave is introduced in the region upstream of the extending point, it would be deformed rapidly in the vicinity of the extending point due to the local scattering effect, leading to an amplitude distortion of the downstream transmitted TS wave. Both mechanisms influence the accumulation of the TS wave and eventually change the transition onset.

The flow field is described by the two-dimensional (2D) Cartesian coordinate system  $(x^*, y^*) = L(x, y)$ , with its origin,  $o$ , locating at the extending point, where  $L$  is selected as the reference length for normalization. In what follows, the asterisk represents the dimensional quantities. The velocity field  $\mathbf{u} = (u, v)$ , pressure  $p$ , density  $\rho$ , temperature  $T$ , and dynamic viscosity  $\mu$  are normalized as

$$(\mathbf{u}, p, \rho, T, \mu) = \left( \frac{\mathbf{u}^*}{u_\infty}, \frac{p^*}{\rho_\infty u_\infty}, \frac{\rho^*}{\rho_\infty}, \frac{T^*}{T_\infty}, \frac{\mu^*}{\mu_\infty} \right), \quad (1)$$

where the subscript  $\infty$  denotes the quantities of the oncoming stream. The time is normalized as  $t = u_\infty t^*/L$ . The flow is controlled by two dimensionless parameters, the Reynolds number  $R$ , and the Mach number  $M$ ,

$$R = \frac{\rho_\infty u_\infty L}{\mu_\infty}, \quad M = \frac{u_\infty}{a_\infty}, \quad (2)$$

where  $a_\infty$  is the sound speed of the free stream. We take  $R \gg 1$ ,  $M < 1$ , and the dimensionless moving speed  $u_s \equiv u_s^*/u_\infty \ll 1$ .

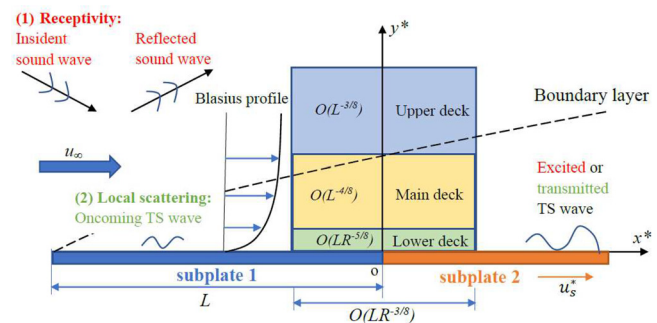


FIG. 1. Sketch of the physical problem and the key scalings.

Particularly, we also assume  $u_s \sim R^{-1/8}$ . For convenience, we introduce  $\epsilon \equiv R^{-1/8} \ll 1$ .

## B. Governing equations

For a perfect-gas flow, the governing equations are the compressible Navier–Stokes (NS) equations

$$\begin{aligned} \frac{\partial \rho}{\partial t} + \nabla \cdot (\rho \mathbf{u}) &= 0, \\ \rho \frac{\partial \mathbf{u}}{\partial t} + \rho(\mathbf{u} \cdot \nabla) \mathbf{u} &= -\nabla p + \frac{2}{R} \nabla \cdot (\mu \mathbf{e}) - \frac{2}{3R} \nabla(\mu \nabla \cdot \mathbf{u}), \\ \rho \frac{\partial T}{\partial t} + \rho(\mathbf{u} \cdot \nabla) T &= (\gamma - 1) M^2 \left[ \frac{\partial p}{\partial t} + (\mathbf{u} \cdot \nabla) p \right] \\ &\quad + \frac{\nabla \cdot (\mu \nabla T)}{\text{Pr} R} + \frac{(\gamma - 1) M^2 \Phi}{R}, \\ \gamma M^2 p &= \rho T, \end{aligned} \quad (3)$$

where the strain rate tensor  $\mathbf{e}$  and the dissipation function  $\Phi$  are expressed as

$$\mathbf{e}_{ij} = \frac{1}{2} \left( \frac{\partial u_i}{\partial x_j} + \frac{\partial u_j}{\partial x_i} \right), \quad \Phi = 2\mu \mathbf{e} : \mathbf{e} - \frac{2}{3} \mu (\nabla \cdot \mathbf{u})^2. \quad (4)$$

$\text{Pr} = 0.72$  is the Prandtl number, and  $\gamma = 1.4$  is the ratio of the specific heat. Here, we choose the Sutherland's viscosity law

$$\mu(T) = \frac{(1 + \bar{C}) T^{3/2}}{T + \bar{C}}, \quad (5)$$

with  $\bar{C} = 110.4/T_\infty$ .

The flow field  $\phi = (\mathbf{u}, p, \rho, T)$  is decomposed into a superposition of a mean flow  $\bar{\phi}$  and an infinitesimal harmonic perturbation  $\tilde{\phi}$ ,

$$\phi(x, y, t) = \bar{\phi}(x, y) + \tilde{\phi}(x, y) e^{-i\hat{\omega}t} + c.c., \quad (6)$$

where  $\hat{\omega}$  is the dimensionless frequency.

## C. Mean flow

The mean-flow quantities  $\bar{\phi}$  are governed by the steady NS equations. The transverse boundary conditions read

$$\bar{u} = H(x)u_s, \quad \bar{v} = 0, \quad \bar{T} = T_w \quad \text{at } y = 0; \quad (7a)$$

$$(\bar{u}, \bar{p}, \bar{\rho}, \bar{T}) \rightarrow (1, 1/(\gamma M^2), 1, 1) \text{ as } y \rightarrow \infty, \quad (7b)$$

where  $H(x)$  is the Heaviside step function and  $T_w$  denotes the dimensionless wall temperature.

At the still part of the plate (subplate 1; but not in the close neighborhood of the extending point  $x=0$ ), the mean flow satisfies the compressible Blasius similarity solution,<sup>14,23</sup>

$$\begin{aligned} &(\bar{u}_B, R^{-1/2} \bar{v}_B, \bar{T}_B, \bar{p}_B, \bar{\rho}_B) \\ &= \left( F'(\eta), R^{-1/2} T(\eta_c F' - F), T(\eta), \frac{1}{T}, \frac{1}{\gamma M^2} \right) + O(R^{-1/2}), \end{aligned} \quad (8)$$

where  $\eta = R^{1/2}(2x)^{-1/2} \int_0^y T^{-1} dy$ ,  $\eta_c = T^{-1} \int_0^\eta T d\eta$ , and prime denotes the derivative with respect to its argument.  $F$  and  $T$  satisfy

$$\begin{aligned} F''' + \frac{FF''}{K} + \frac{K'T'F''}{K} &= 0, \\ T'' + \text{Pr} \frac{FT'}{K} + \frac{K'T'^2}{K} + \text{Pr}(\gamma - 1)M^2 F'^2 &= 0, \end{aligned} \quad (9)$$

which are subject to the boundary conditions  $F(0) = F'(0) = 0$ ,  $T(0) = T_w$  and  $(F', T) \rightarrow 1$  as  $\eta \rightarrow \infty$ , where  $K = \mu/T$ .

At the moving plate (subplate 2) sufficiently downstream of the extending point, the mean-flow quantities also satisfy (9), but the no-slip condition is replaced by  $F'(0) = u_s$ .

In the vicinity of the extending point,  $x=0$ , the discontinuity of the wall boundary condition (7a) induces a rapid distortion of the mean flow, leading to the emergence of the viscous lower deck. This can be mathematically described by the triple-deck theory.<sup>24,25</sup> Following these papers, we know that for  $R \gg 1$ , the thicknesses of the lower, main, and upper decks are  $O(\epsilon^5 L)$ ,  $O(\epsilon^4 L)$ , and  $O(\epsilon^3 L)$ , respectively, and the streamwise length scale of the triple-deck region is  $O(\epsilon^3 L)$ .

Now we rescale the coordinate system and flow field in the lower deck, which are expressed as<sup>13,14</sup>

$$\begin{cases} X = \lambda^{5/4} (1 - M^2)^{3/8} C^{-3/8} T_w^{-3/2} \epsilon^{-3} x, \\ Y = \lambda^{3/4} (1 - M^2)^{1/8} C^{-5/8} T_w^{-3/2} \epsilon^{-5} y, \\ (\bar{U}, U_s) = \lambda^{-1/4} (1 - M^2)^{1/8} C^{-1/8} T_w^{-1/2} \epsilon^{-1} (\bar{u}, u_s), \\ \bar{V} = \lambda^{-3/4} (1 - M^2)^{-1/8} C^{-3/8} T_w^{-1/2} \epsilon^{-3} \bar{v}, \\ \bar{P} = \lambda^{-1/2} (1 - M^2)^{1/4} C^{-1/4} \epsilon^{-2} [\bar{p} - 1/(\gamma M^2)], \end{cases} \quad (10)$$

where  $\lambda = (\mu_w T_w)^{1/2} \bar{u}_{B,\bar{y}}|_{\bar{y}=0}$  is the wall shear of the Blasius solution with  $\bar{y} = R^{1/2} y$  and  $\mu_w = \mu(T_w)$ , and  $C = \mu_w/T_w$ . Note that the effect of the non-parallelism is  $O(R^{-1/2})$ , which is much smaller than the terms of our interest. The temperature and density distortions do not appear in the leading-order equations, rendering an incompressible nature of the lower deck. Substituting into the NS equations and retaining the leading-order terms, we obtain the nonlinear boundary-layer equations

$$\bar{U}_X + \bar{V}_Y = 0, \quad \bar{U} \bar{U}_X + \bar{V} \bar{U}_Y = -\bar{P}_X + \bar{U}_{YY}, \quad P_Y = 0. \quad (11)$$

They are subject to boundary conditions

$$\bar{U}(X, 0) = H(X)U_s, \quad \bar{V}(X, 0) = 0; \quad (12)$$

$$\begin{aligned} \bar{U}(X, Y) &\rightarrow Y + \bar{A}(X) \quad \text{as } Y \rightarrow \infty; \\ (\bar{U}, \bar{V}, \bar{A}, \bar{P}) &\rightarrow (Y, 0, 0, 0) \quad \text{as } X \rightarrow -\infty; \\ \bar{A} &\rightarrow U_s \quad \text{as } X \rightarrow \infty, \end{aligned} \quad (13)$$

where  $\bar{A}(X)$  is named as the displacement function of the mean flow. The above system is, however, not closed, which requires an additional condition by matching with the upper-deck solutions through the main deck. By doing this, we obtain the pressure-displacement law

$$\bar{P} = \frac{1}{\pi} \int_{-\infty}^{\infty} \frac{\bar{A}_\xi}{X - \xi} d\xi, \quad (14)$$

where the integral is of Cauchy principle value. For  $U_s \ll 1$ , this system can be solved analytically, but for  $U_s = O(1)$ , the numerical approaches as in Refs. 12–14, and 16 need to be employed.

#### D. Perturbation evolution around the extending point

The lower-deck perturbation velocity field  $\tilde{U}$  and pressure  $\tilde{P}$  are normalized by the same scalings as (10). Because the characteristic TS frequency is  $O(\epsilon^2 u_\infty/L)$ ,<sup>26</sup> we rescale the time and frequency as

$$\left(\tilde{t}, \frac{1}{\tilde{\omega}}\right) = \frac{\lambda^{3/2}(1-M^2)^{1/4}C^{-1/4}T_w^{-1}u_\infty}{\epsilon^2 L} \left(t, \frac{1}{\tilde{\omega}}\right). \quad (15)$$

Thus, the lower-deck governing equations for the perturbation field read

$$\begin{aligned} \tilde{U}_X + \tilde{V}_Y &= 0, \quad \tilde{P}_Y = 0, \\ -i\omega\tilde{U} + \tilde{U}\tilde{U}_X + \tilde{U}_X\tilde{U} + \tilde{V}\tilde{U}_Y + \tilde{U}_Y\tilde{V} &= -\tilde{P}_X + \tilde{U}_{YY}, \end{aligned} \quad (16)$$

which are subject to the transverse boundary conditions

$$\tilde{U}(X, 0) = \tilde{V}(X, 0) = 0, \quad \tilde{U}(X, \infty) \rightarrow \tilde{A}, \quad (17)$$

and the pressure-displacement relation

$$\tilde{P} = \frac{1}{\pi} \int_{-\infty}^{\infty} \frac{\tilde{A}_\xi}{X - \xi} d\xi, \quad (18)$$

where the displacement function  $\tilde{A}$  characterizes the perturbation amplitude.

In the upstream limit, the perturbation field is selected according to the physical problem of interest. For the receptivity problem, the upstream perturbation is a Stokes-layer wave induced by a freestream acoustic wave, whereas for the local scattering problem, the upstream perturbation is a TS wave. Their profiles are introduced in Subsections II E and II F.

#### E. Boundary-layer response to freestream acoustic waves

Assume the incident acoustic wave to propagate with a frequency  $\omega^*$  and streamwise and wall-normal wavenumbers  $k_x^*$  and  $k_y^*$ , respectively; then, the pressure field can be expressed as

$$p_a^* = \mathcal{E}_a(e^{ik_y^*y^*} + C_R e^{-ik_y^*y^*})e^{i(k_x^*x^* - \omega_a^*t^*)} + c.c., \quad (19)$$

where  $t^*$  is the time,  $\mathcal{E}_a$  is the acoustic amplitude, and  $C_R$  is the reflection coefficient. The incident angle of the acoustic wave is defined as  $\theta = \tan^{-1}(k_y^*/k_x^*)$ . According to the acoustic-wave dispersion relation (obtained from the linearized Euler equations in the upper deck), we obtain that its phase speed

$$c_a^* = u_\infty [1 \pm (M \cos \theta)^2], \quad (20)$$

where the plus and minus signs represent the fast (downstream-propagating) and slow (upstream-propagating) acoustic waves, respectively.

Applying the transverse momentum equation at the bottom of the upper deck and taking into account the non-penetration condition, we obtain that the transverse pressure gradient should vanish. This leads to  $C_R = 1$  for  $\theta \neq 0$ , implying an rigid reflection nature.

Because we are focusing on the receptivity of the TS waves by acoustic forcing, the characteristic acoustic frequency should agree with the TS frequency, and so  $\omega_a^* \sim \epsilon^2 u_\infty/L$ . It is seen from (20) that the acoustic speed  $c_a^* \sim u_\infty$ , therefore,  $k_x^* \sim \epsilon^2/L$ , indicating the long-wavelength nature of the freestream acoustic waves of interest.

According to the lower-deck scalings (10), the dimensionless streamwise wavenumber is

$$k_x = \epsilon \lambda^{-5/4} (1 - M^2)^{-3/8} T_w^{3/2} k_x^* L. \quad (21)$$

In the lower deck, the freestream acoustic wave drives an unsteady Stokes-layer wave, whose perturbation profiles, under the normalization (10), are expressed as<sup>3</sup>

$$(U_a, V_a, P_a) = 2\mathcal{E}_a C_p \epsilon^{-1} \left(\frac{k_x}{\omega} \hat{U}_a, 0, \epsilon^{-1}\right) e^{i(\epsilon k_x X - \omega t)} + \dots, \quad (22)$$

where  $C_p = \lambda^{-1/2} (1 - M^2)^{1/4} C^{-1/4}$ , and  $\hat{U}_a = 1 - e^{-(i\omega)^{1/2} Y}$ . Note that the wavenumber  $\epsilon k_x$  indicates that the wavelength of the acoustic wave is much greater than the streamwise length scale of the triple-deck region and so can be considered as an  $X$ -invariant perturbation to leading-order accuracy. Additionally, it is also seen that  $U_a$  and  $P_a$  are  $O(\epsilon^{-1})$  and  $O(\epsilon^{-2})$ , respectively; however, this does not mean that these quantities vary their magnitude in the lower deck, because their scalings are rescaled according to (10). At the moving wall, the leading-order solution (22) is also valid because the no-slip condition for the perturbation field at the wall does not change.

#### F. TS waves

According to Refs. 26 and 12, we can express the TS wave in the lower deck as

$$\mathcal{E}(U_s, V_s, P_s) e^{i(\alpha X - \omega t)} + c.c., \quad (23)$$

where  $\alpha = \alpha_r + i\alpha_i$  is the dimensionless complex wavenumber with the opposite of its imaginary part  $-\alpha_i$  denoting its growth rate and  $\mathcal{E}$  characterizes its amplitude. All the quantities are rescaled under the lower-deck scalings. At the still wall, their solutions are<sup>12</sup>

$$\begin{aligned} U_s &= \hat{q} \int_{\zeta_0}^{\zeta} \text{Ai}(\zeta') d\zeta', \\ V_s &= -(i\alpha)^{2/3} \hat{q} \int_{\zeta_0}^{\zeta} (\zeta' - \zeta_0) \text{Ai}(\zeta') d\zeta', \quad P_s = \alpha, \end{aligned} \quad (24)$$

where  $\zeta = (i\alpha)^{1/3} Y + \zeta_0$ ,  $\hat{q} = [\int_{\zeta_0}^{\infty} \text{Ai}(\zeta') d\zeta']^{-1}$ ,  $\zeta_0 = -i\omega(i\alpha)^{-2/3}$ , and  $\text{Ai}$  is the Airy function of the first kind.<sup>27</sup> Its dispersion relation is

$$\Delta(\omega, \alpha) = (i\alpha)^{1/3} \alpha \int_{\zeta_0}^{\infty} \text{Ai}(\zeta') d\zeta' - \text{Ai}'(\zeta_0) = 0. \quad (25)$$

If the wall is extending, the base flow  $(\bar{U}, \bar{V}) \rightarrow (Y + U_s, 0)$  as  $X \rightarrow \infty$ . The above dispersion relation is also valid, but with  $\omega$  being replaced by  $\omega - \alpha U_s$ . This indicates that the moving wall induces a Doppler effect, for which the TS frequency is shifted due to the relative phase speed with respect to the moving wall. In the following, we denote the downstream TS wavenumber and eigenfunctions as  $\alpha_1$  and  $(U_{s1}, V_{s1}, P_{s1})$ , respectively. Thus, for the scattering calculations, the upstream perturbations are selected from (24), while the downstream perturbations have a dispersion relation  $\Delta(\omega - \alpha_1 U_s, \alpha_1) = 0$ .

#### G. Receptivity and transmission coefficients

##### 1. Calculation of the receptivity coefficient

In the receptivity process, the perturbation profiles in the upstream and downstream limits are predicted as



$$(\tilde{U}, \tilde{V}, \tilde{P}_X) \rightarrow (\hat{U}_a, 0, i\omega) + \cdots \quad \text{as } X \rightarrow -\infty, \quad (26)$$

$$(\tilde{U}, \tilde{V}, \tilde{P}_X) \rightarrow \mathcal{A}(U_{s1}, V_{s1}, i\alpha_1^2 X) e^{i\alpha_1 X} + (\hat{U}_a, 0, i\omega) + \cdots \quad \text{as } X \rightarrow \infty, \quad (27)$$

where  $\mathcal{A}$  measures the velocity amplitude of the excited TS wave.

The receptivity calculation is conducted by solving numerically (16) with (17), (18), (26), and (27). The computational domain should include the extending point,  $X=0$ , such that the rapid deformation of the perturbations due to the scattering effect is well calculated. This system is somewhat similar to the receptivity of the wake modes to freestream acoustic waves in the trailing-edge flow as in Ref. 28, and so following that paper, we can discretize this linear system into a high-dimensional linear-equation system,

$$\mathbf{A}\tilde{\phi} = \mathbf{b}, \quad (28)$$

where  $\tilde{\phi}$  is the unknown vector consisting of the perturbation field and the amplitude  $\mathcal{A}$  and  $\mathbf{A}$  and  $\mathbf{b}$  can be found in Appendix A 2 of Ref. 28.

When  $\mathcal{A}$  is obtained, we can predict the pressure perturbation of the excited TS wave to be  $\alpha_1 \mathcal{A}$  in the downstream limit. According to (22), for an incident acoustic wave with a pressure-amplitude of  $\mathcal{E}_a$  and a non-zero incident angle, the amplitude of the Stokes-layer wave should be  $2\mathcal{E}_a C_p \epsilon^{-1} k_x / \omega$ . Therefore, the receptivity efficiency  $\mathcal{H}$ , defined by the pressure amplitude of the excited TS wave to that of the incident acoustic wave, is expressed as

$$\mathcal{H} = 2\epsilon^{-1} C_p k_x \frac{\alpha_1}{\omega} \mathcal{A}. \quad (29)$$

It is noted that the large prefactor  $\epsilon^{-1}$  is due to the mismatch of the magnitudes of the pressure and streamwise velocity perturbations between the acoustic and the TS dispersion relations, i.e., for the acoustic signature,  $p_a^*$  and  $u_a^*$  are of the same order, whereas for the TS wave,  $p_s^*$  is  $O(\epsilon)$  smaller than  $u_s^*$ . It is easy seen that the receptivity coefficient is dependent on three factors, namely, the base-flow effect  $C_p$ , the acoustic-forcing effect  $k_x$ , and the instability property  $\alpha_1 \mathcal{A} / \omega$ . The former two factors are determined when the physical problem is fixed and our task is to solve for the third factor from (28). Therefore,  $\mathcal{A}$  is also interpreted as the efficiency function of the receptivity process.

Remarkably, if  $U_s \ll 1$ , then the receptivity coefficient can be obtained analytically, as shown in Appendix. Comparing (27) with (A8), we find that the efficiency function  $\mathcal{A}$  for the linear case is predicted by  $U_s \mathcal{A}_1$  with  $\mathcal{A}_1$  being defined in (A9).

## 2. Calculation of the transmission coefficient

In the scattering calculation, the upstream perturbation field behaves like

$$(\tilde{U}, \tilde{V}, \tilde{P}) \rightarrow (U_s, V_s, P_s) e^{i\alpha X} \quad \text{as } X \rightarrow -\infty. \quad (30)$$

while, in the downstream limit, the perturbation displacement function behaves like

$$(\tilde{U}, \tilde{V}, \tilde{P}) \rightarrow \mathcal{T}(U_{s1}, V_{s1}, P_{s1}) e^{i\alpha_1 X} \quad \text{as } X \rightarrow \infty, \quad (31)$$

where  $\mathcal{T}$  is the transmission coefficient characterizing the amplitude of the transmitted TS wave.  $\mathcal{T}$  may be used as a systematic parameter leading to the quantitative change in the transition onset.

The perturbation field can be described quantitatively by the local scattering framework.<sup>12</sup> That paper was focusing on the impact of local roughness on TS instability, and because the upstream and downstream perturbations are of the same form to leading order, a generalized eigenvalue system was developed. However, in the present paper, the downstream TS wave shows different eigenfunctions from the upstream TS wave due to the Doppler effect, and so the generalized eigenvalue system as in Ref. 12 is not valid. Fortunately, the high-dimensional linear-equation system as in (28) is also valid for the local scattering problem, and the same numerical approach as for the receptivity calculations is employed. It is noted that if  $U_s \ll 1$ , the transmission coefficient  $\mathcal{T}$  to the leading order is exactly unity.

## III. NUMERICAL RESULTS

### A. Mean flow

The numerical approaches and the code for solving the nonlinear lower-deck Eq. (11) with (12)–(14) are the same as those in Refs. 12–14. Due to the rescaling (10), the lower-deck system is independent of  $M$ ,  $R$ , and  $T_w$ , and the only controlling parameter is  $U_s$ . For the calculation of the base flow, the computational domain is  $[-50, 50] \times [0, 10]$ , and non-uniform grid points that are clustered near  $X=0$  and  $Y=0$  are employed, with its number of  $1001 \times 31$ . Sufficient resolution has been confirmed. Figure 2 shows the contours of the mean shear  $\bar{U}_Y$  in the close neighborhood of the extending point. In the upstream locations, the mean shear is unity, agreeing with the Blasius solution. As the extending point is approached,  $\bar{U}_Y$  in the near-wall region increases remarkably. After passing over the extending point, a low shear region is observed, followed by a gradual increase in  $\bar{U}_Y$ , approaching the downstream asymptote  $\bar{U}_Y \rightarrow 1$  as indicated in (12) and (13).

Figure 3 plots the streamwise evolution of the normalized mean pressure  $\bar{P}/U_s$  and displacement function  $\bar{A}/U_s$  for different  $U_s$  values. The mean pressure is zero at sufficiently upstream locations and decreases as the extending point is approached. A drastic increase in  $\bar{P}$  is observed immediately downstream of  $X=0$ , followed by a mild decrease, which approaches zero in the downstream limit. The displacement function  $\bar{A}$ , on the contrary, increases with  $X$  monotonically, and the increment is rather remarkable in the close neighborhood of  $X=0$ . For  $U_s \ll 1$ , both  $\bar{P}$  and  $\bar{A}$  increase with  $U_s$  linearly, leading to

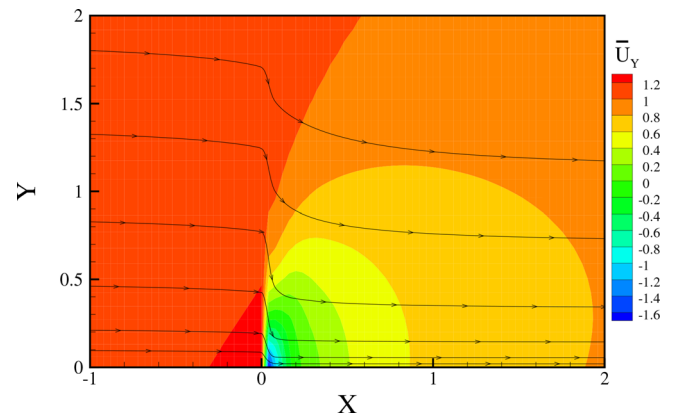
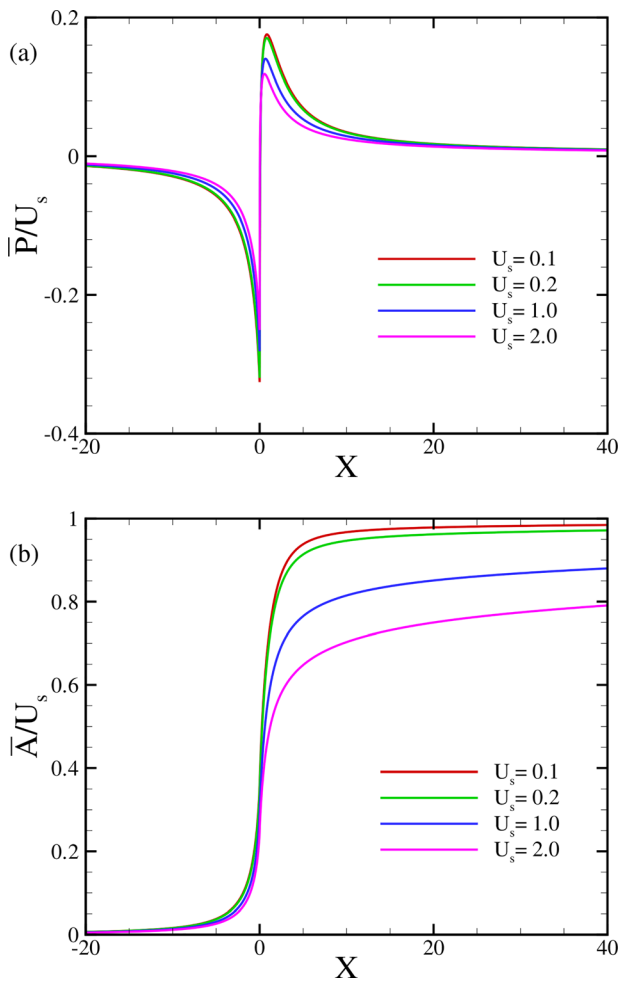


FIG. 2. Contours of the mean shear  $\bar{U}_Y$  and the streamlines for  $U_s = 1$ .



**FIG. 3.** Streamwise evolution of mean pressure (a) and displacement function (b) normalized by the moving-wall speed.

an almost overlap of  $\bar{P}/U_s$  and  $\bar{A}/U_s$ , shown by the red and green lines. When  $U_s = O(1)$ , both  $\bar{P}/U_s$  and  $\bar{A}/U_s$  are smaller than the linear cases and increase in  $U_s$  leads to a decrease in the values. This indicates that the nonlinearity suppresses the strength of the mean-flow distortion.

### B. TS instability

The solutions of the TS dispersion relation (25) for a still wall are shown in Fig. 4(a). The wavenumber increases with  $\omega$  monotonically, and the increasing rate shows an apparent change at around  $\omega = 1$ . The TS wave is stable for small frequencies and becomes neutral at  $\omega = 2.3$ . It increases with  $\omega$  until the most unstable frequency,  $\omega = 7.25$ , after which the growth rate reduces. In the following calculations of the receptivity and local scattering regimes, we are interested in the unstable frequency band, namely,  $\omega \geq 2.3$ .

When the wall is extending at  $U_s = 1.0$ , the dispersion relation is changed, as shown in Fig. 3(b). Due to the Doppler effect, the neutral frequency and the most unstable frequency are shifted to  $\omega = 3.3$  and

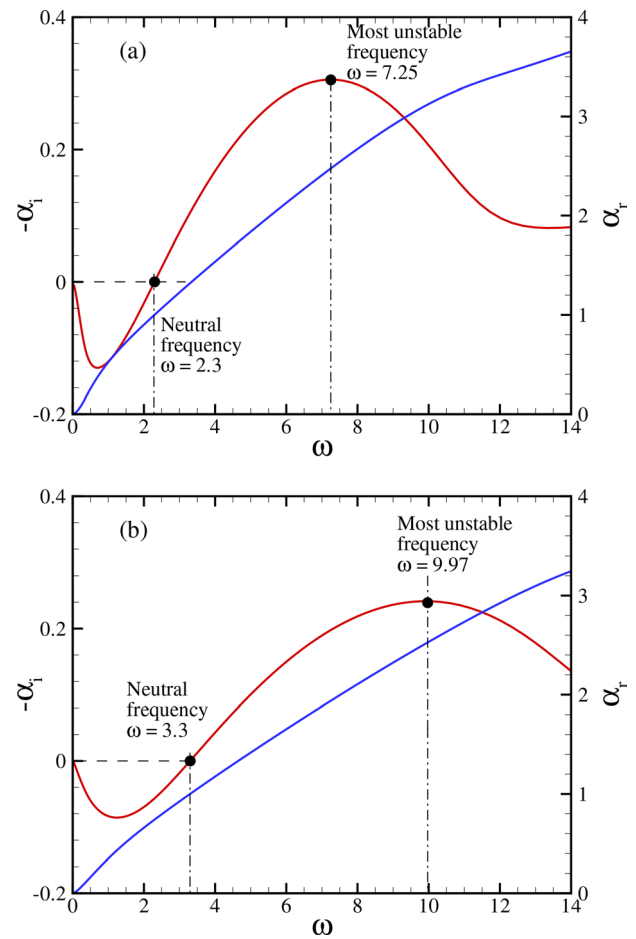


**FIG. 4.** Dependence on the frequency  $\omega$  of the growth rate  $-\alpha_i$  and wavenumber  $\alpha_r$  of the TS wave for  $U_s = 0$  (a) and 1.0 (b).

9.97, respectively, with the growth rate of the most amplified TS being reduced to 0.24. Thus, it is convenient to introduce a factor to quantify the difference of the growth rate between the moving and still walls,  $\Delta_{xi}(\omega, U_s) \equiv \alpha_i(\omega, U_s) - \alpha_i(\omega, 0)$ , whose values for three representative  $U_s$  values are shown in Fig. 5. In the frequency bands,  $\omega \in [1.35, 8.89]$ ,  $[1.49, 9.45]$ , and  $[1.69, 10.35]$ ,  $\Delta_{xi} < 0$ , indicating the stabilizing effect of the moving wall for  $U_s = 0.5, 1.0$  and 2.0, respectively, while in the rest frequency bands, the moving wall plays a destabilizing role. We are focusing on the behavior of the unstable TS waves, so the destabilizing frequency band for  $\omega < 2$  is not of interest. Therefore, the critical frequency separating the stabilizing and destabilizing effects for  $U_s = 0.5, 1.0$ , and 2.0 is 8.89, 9.45, and 10.35, respectively, showing an increasing trend of a higher moving speed.

### C. TS receptivity calculation

For the receptivity calculations, we introduce a Stokes-layer wave (26) as the inflow perturbation and solve for the perturbation field  $\tilde{\phi}$  from the linear system (28). The receptivity coefficient  $\mathcal{R}$  is easy to be obtained from (29) as long as the efficiency function  $\mathcal{A}$  is determined

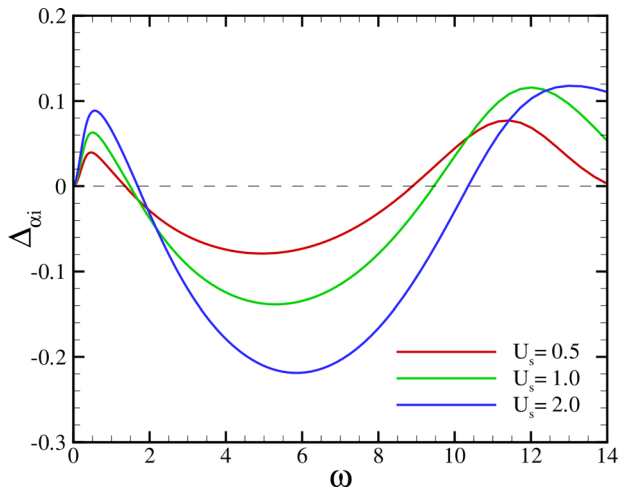


**FIG. 5.** The difference of the TS growth rate of the moving wall from that of the still wall  $\Delta\alpha_i$ .

from the downstream perturbation asymptote. Note that for the calculation of the perturbation evolution, the computational domain is changed to be  $[-7.5, 15] \times [0, 10]$ , with the number of grid points  $1501 \times 51$ .

The contours of the perturbation field  $Re[\tilde{A}_Y]$  for  $\omega = 6$  and  $U_s = 1$  are shown in Fig. 6(a), where  $Re$  represents the real part. Upstream of the extending point, the Stokes-layer wave shows zero gradient in the streamwise direction due to its long-wavelength nature. After propagating over the extending point, the perturbation profile undergoes a rapid distortion, showing an oscillatory nature in the  $X$  direction with its amplitude growing drastically. If the Stokes-layer wave  $\tilde{U}_a$  is subtracted out from the perturbation field, shown in panel (b), the downstream exponentially growing feature is clearly exhibited.

The dependence of the receptivity efficiency function  $|A|$  on the acoustic frequency  $\omega$  is plotted by the solid curves in Fig. 7(a). Overall,  $A$  decreases with  $\omega$  monotonically, showing a stronger receptivity near the lower-branch neutral point of the TS wave. The implication is that such a strong receptivity effect induces a relatively large initial amplitude of the lower-branch neutral TS wave, which further experiences a long-distance accumulation and possibly leads to transition at a certain downstream location. The faster the moving speed  $U_s$  is, the stronger the receptivity efficiency would be. Comparing with (29), it is seen that the receptivity coefficient also depends on a few other factors. Usually,  $\alpha_1/\omega$  does not vary much, as shown in Fig. 4. Increasing the Reynolds number (so decreasing  $\epsilon$ ),  $C_p = \lambda^{-1/2}(1 - M^2)^{1/4}C^{-1/4}$  (decreasing  $\lambda$ ,  $M$ , and  $T_w$ ), and the streamwise wavenumber of the acoustic wave also leads to a stronger receptivity coefficient. The linear prediction of the efficiency function  $A = U_s A_1$ , with  $A_1$  defined in (A9), is also shown for comparison. The agreement for  $U_s = 0.5$  is satisfactory, whereas for higher extending speeds, the linear theory underpredicts the receptivity efficiency.

In Fig. 7(b), we plot the dependence of  $|A|$  on  $U_s$  for three representative frequencies, where the linear predictions are also plotted by the dot-dashed lines. As expected, the receptivity efficiency is well predicted by the linear theory when  $U_s$  is slower than about 0.5, whereas it increases superlinearly with  $U_s$  for higher  $U_s$  values.

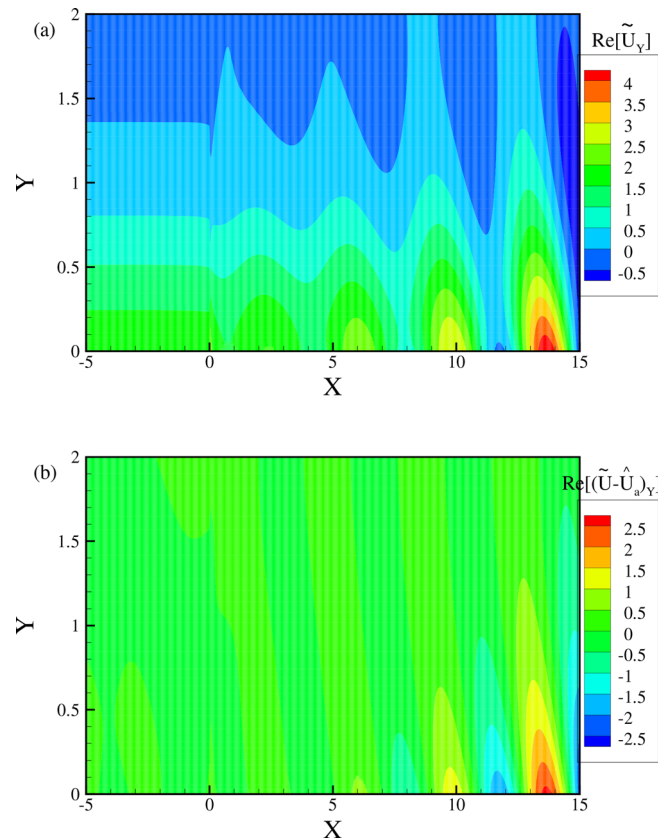


**FIG. 6.** Contours of the real parts of the perturbation field  $Re[\tilde{A}_Y]$  (a) and the excited perturbation field  $Re[(\tilde{U} - \tilde{U}_a)_Y]$  (b) for  $\omega = 6$  and  $U_s = 1$  for the receptivity regime.

## D. TS scattering calculation

In this subsection, we introduce an oncoming TS wave (30) as the inflow perturbation and also solve the linear equation system (28) numerically. Both the perturbation field and the transmission coefficient are obtained. For demonstration, Fig. 8(a) plots the evolution of the perturbation amplitude  $A$  for  $\omega = 6$  and  $U_s = 1$ . The perturbation shows an oscillatory nature in the streamwise direction, whose amplitude grows exponentially as propagating downstream. In the upstream limit, the perturbation amplitude agrees with the oncoming TS evolution,  $e^{iz_1 X}$ , shown by the blue dashed line, whereas in the downstream limit, it approaches the transmitted TS evolution,  $\mathcal{T} e^{iz_1 X}$ , shown by the pink dot-dashed line. Apparently, these two asymptotic curves show different growing trends, because the TS growth rate on the moving wall is distorted; see Fig. 4. Moreover, at the extending point, the two asymptotic curves show different values. We introduce the transmission coefficient  $\mathcal{T}$  to quantify the ratio of the amplitude of the downstream asymptote at  $X=0$  to that upstream, namely,  $\mathcal{T} = A_2/A_1$ . Note that both  $A_1$  and  $A_2$  are complex, so is  $\mathcal{T}$ . For this case, it is calculated that  $|\mathcal{T}| \approx 1.69$ , indicating an amplification of the amplitude at  $X=0$  due to the scattering effect. However, the overall impact of the moving wall is stabilizing for  $X > 4.0$ , because there is a continuous suppress effect on the local growth rate induced by the wall extending.



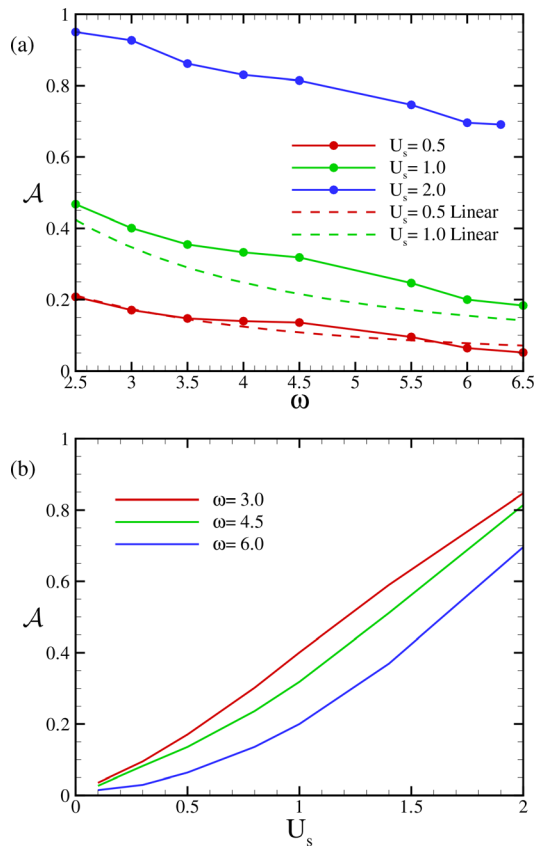


FIG. 7. Dependence of the receptivity efficiency  $\mathcal{A}$  on  $\omega$  (a) and  $U_s$  (b).

Note that at a finite Reynolds number, the downstream development is always accompanied by the growth of the local boundary-layer thickness, leading to the increase in the local frequency. When the local frequency is above the most unstable frequency, the aforementioned suppress effect of the moving wall may be changed to an enhancement effect, and so a successive destabilizing effect could be met in the further downstream locations.

If, on the contrary, the local frequency  $\omega$  is increased to a higher value, then the TS growth rate at the moving wall may become greater than that at the still wall, as shown in Fig. 5. Figure 8(b) shows an example for the evolution of the TS wave at  $\omega = 10$ . Both the local scattering effect and the local growth-rate correction due to the moving wall destabilize the TS wave. The implication is that when the extending point is placed in a downstream location, the overall destabilizing effect becomes greater. Since the local growth-rate correction is easily to be predicted by the Orr–Sommerfeld equations under the parallel-flow assumption, we will focus on the local scattering calculations in the following.

Figure 9 compares the perturbation profiles normalized by their amplitudes,  $|\tilde{U}|/\tilde{A}$ . The unperturbed TS profile is almost sustained until the extending point,  $X = 0$ . However, in the locations downstream of the extending point, the profile varies rather drastically and approaches the downstream eigenfunction  $U_{s1}$  asymptotically.

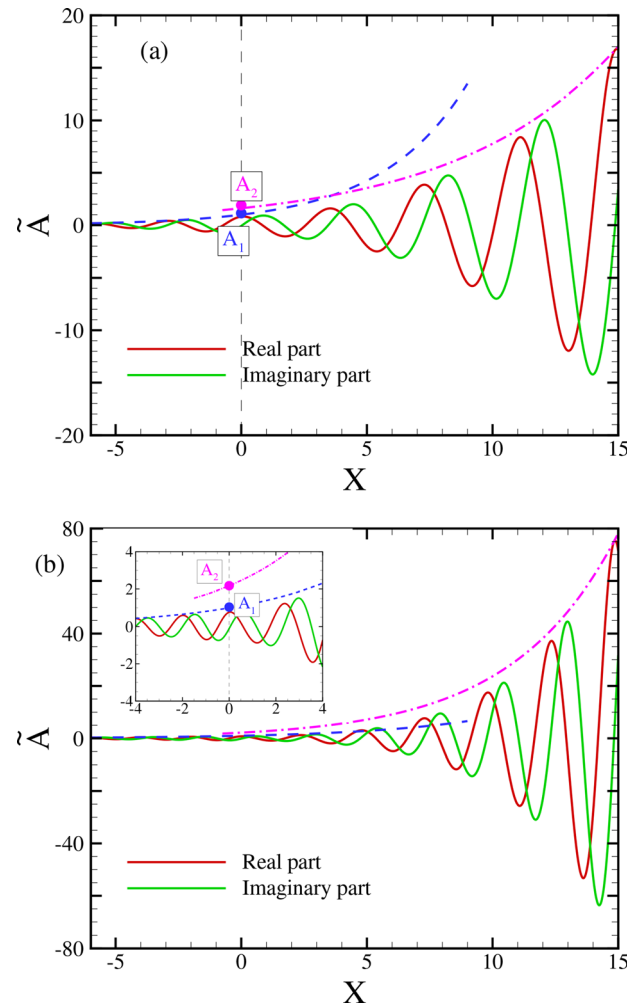
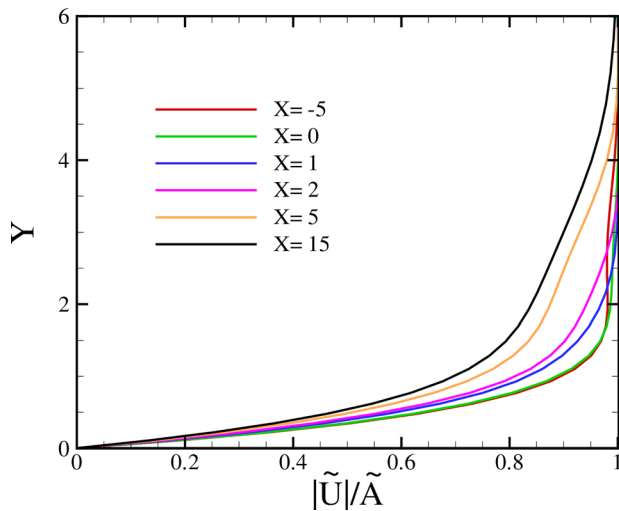


FIG. 8. Evolution of the perturbation amplitude  $\tilde{A}$  for  $\omega = 6$  (a) and  $10$  (b), with  $U_s = 1$  for the local scattering regime. The blue dashed and pink dot-dashed lines denote the upstream and downstream asymptotes of the amplitude.

Figure 10 plots the dependence of the transmission coefficient  $\mathcal{T}$  on  $\omega$  and  $U_s$  for representative cases.  $|\mathcal{T}|$  is greater than unity for all the frequencies and extending-wall speed, indicating the overall destabilizing effect of the local scattering process. As  $U_s \rightarrow 0$ , the transmission coefficient approaches unity, agreeing with the linear limit, whereas for a moderator  $U_s$ , the scattering effect measured by  $|\mathcal{T}| - 1$  increases superlinearly with  $U_s$ .  $|\mathcal{T}|$  increases with  $\omega$  monotonically, confirming that applying the extending wall to a downstream position may induce a relatively greater destabilizing effect. This effect, combined with the local growth-rate correction, could lead to premature of transition to turbulence eventually.

#### IV. CONCLUDING REMARKS

In this paper, we study the effect of the surface morphing of an extensible flat plate on the subsonic-boundary-layer TS instabilities using a large-Reynolds-number asymptotic approach. Two relevant mechanisms are considered, namely, the local receptivity



**FIG. 9.** Normalized perturbation profiles  $|\tilde{U}|/\tilde{A}$  at different streamwise stations for  $\omega = 6$  and  $U_s = 1$ .

and the local scattering mechanisms, both of which could influence the transition onset to turbulence by affecting the excitation and evolution of TS modes in boundary layers. Physically, these two mechanisms are dependent on quite a few controlling parameters, including the Mach number, the Reynolds number, the wall temperature, the moving speed of the extending wall, and the frequency of the introduced perturbations (freestream acoustic or oncoming TS waves). However, in the asymptotic framework, only two parameters, namely, the dimensionless frequency  $\omega$  and the wall-extending speed  $U_s$ , remain, which reduces greatly the complexity of the system and enables a systematic study to visit the complete parameter space.

In the close neighborhood of the extending point, the discontinuity of the boundary conditions at the wall leads to the emergence of the triple-deck region in which a self-induced pressure gradient appears. Solving numerically the lower-deck nonlinear boundary-layer equations closed by the pressure-displacement relation, we are able to quantitatively describe the rapidly distorted mean flow. The dispersion relation of the TS instability at the moving wall shares the same feature with that at the still wall, but a Doppler effect is observed such that the phase speed undergoes a shift due to the moving speed.

If a Stokes-layer wave driven by freestream acoustic wave is introduced upstream of the extending point, then the TS wave could be generated due to the receptivity regime. Solving numerically this linear system, we obtain the receptivity efficiency function for different frequencies and moving speeds. Overall, the local receptivity is stronger for a lower-frequency acoustic forcing and a higher moving speed, and the receptivity calculations approach the linear prediction when  $U_s$  is sufficiently small ( $U_s$  is less than about 0.5). Because in this paper the frequency is normalized by the local boundary-layer thickness, the downstream development of the perturbations would be accompanied by an increase in the dimensionless frequency. Thus, the local receptivity is more important if the extending point is arranged in an upstream location.

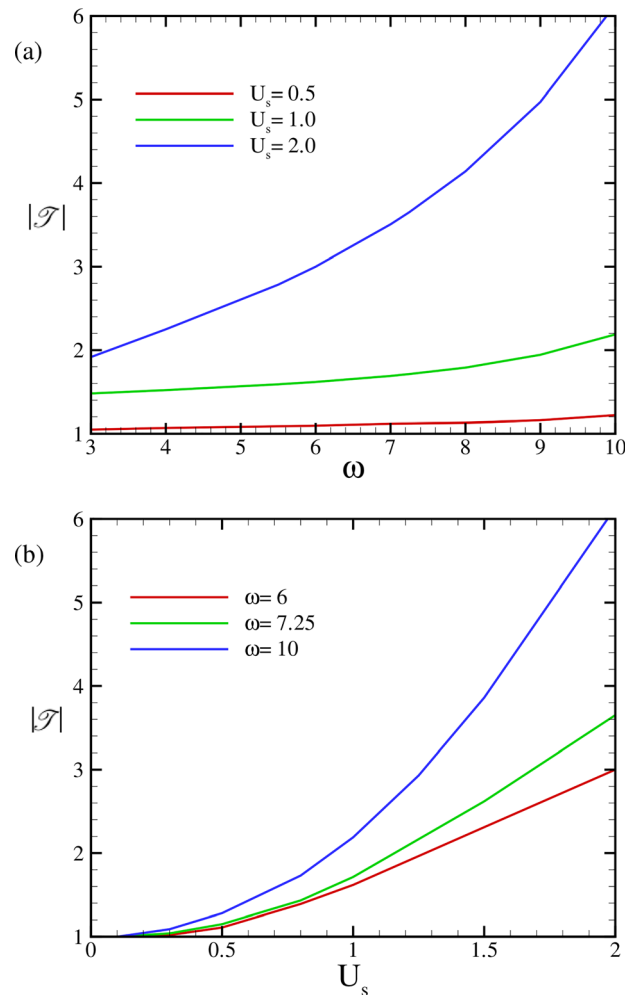


**FIG. 10.** Dependence of the transmission coefficient  $\mathcal{T}$  on  $\omega$  (a) and  $U_s$  (b).

The scattering calculations are performed by introducing the oncoming TS waves from the upstream limit. Actually, the TS amplitude development relies on two factors, the local scattering effect and the modification of the local growth rate due to the continuously moving wall. The latter is easy to be predicted by solving locally the instability equation, i.e., either the Orr-Sommerfeld equation at a finite Reynolds number or the dispersion relation (25) in the asymptotic viewpoint. It is seen from Fig. 5 that for each  $U_s$ , there exists a critical frequency, above and below which the moving wall plays a stabilizing effect and a destabilizing effect, respectively. The local scattering effect is quantified by the transmission coefficient, which is always above unity for all frequencies and moving speeds, indicating a destabilizing effect. In contrast to the receptivity regime, the transmission coefficient increases monotonically with the frequency. Combining both the growth-rate correction and the local scattering effects, we find that if the surface extending point of the moving wall is arranged sufficiently downstream, a rather strong destabilizing effect would appear, leading to premature of transition to turbulence eventually.

## ACKNOWLEDGMENTS

This research was supported by the National Key R&D Program of China (Grant No. 2021YFA0719200), NSFC (Grant Nos. U20B2003, 11988102, and 91952202), and Strategic Priority Research Program, CAS (Grant No. XDB22040104).

## AUTHOR DECLARATIONS

## Conflict of Interest

The authors have no conflicts to disclose.

## Author Contributions

**Ming Dong:** Conceptualization (lead); Data curation (lead); Formal analysis (lead); Funding acquisition (lead); Investigation (lead); Methodology (lead); Project administration (lead); Resources (lead); Software (lead); Supervision (lead); Validation (lead); Visualization (lead); Writing – original draft (lead); Writing – review and editing (lead).

## DATA AVAILABILITY

The data that support the findings of this study are available from the corresponding author upon reasonable request.

APPENDIX: RECEPTIVITY FOR SMALL MOVING SPEED  $U_s \ll 1$ 

The flow field  $\phi = (U, V, P)$  in the lower deck can be expressed as the superposition of the base flow, the mean-flow distortion  $\bar{\phi}_1$ , the Stokes-layer  $\phi_a$ , and the excited perturbation  $\tilde{\phi}$ ,

$$\phi = (Y, 0, 0) + U_s \bar{\phi}_1 + \mathcal{E}_a(\phi_a(Y)e^{ik_x X} + U_s \tilde{\phi}_1(X, Y) + \dots)e^{-i\omega t} + c.c.. \quad (A1)$$

We may describe the flow field by performing Fourier transform with respect to  $X$ ,

$$(\bar{\phi}_2, \tilde{\phi}_2)(k, Y) = \frac{1}{\sqrt{2\pi}} \hat{f}^{-1}(k) \int_{-\infty}^{\infty} (\bar{\phi}_1, \tilde{\phi}_1)(X, Y)e^{-ikX} dX, \quad (A2)$$

where the factor  $\hat{f}(k)$  denotes the Fourier transform of the Heaviside step function,  $\hat{f}(k) = \sqrt{\frac{\pi}{2}}\delta(k) + \frac{1}{\sqrt{2\pi}ik}$ . Note that the factor  $\hat{f}(k)$  appears because both  $\bar{\phi}_2$  and  $\tilde{\phi}_2$  are linearly dependent on it.

The mean-flow distortion satisfies

$$ikY\bar{U}_{2,Y} = \bar{U}_{2,YY}; \quad \bar{U}_2(k, 0) = 1, \quad (A3)$$

$$ik\bar{P}_2 = \bar{U}_{2,YY}(k, 0), \quad \bar{U}_2(k, \infty) \rightarrow \bar{P}_2/k.$$

The solutions, combined with the continuity equation, are

$$\bar{U}_2 = 1 - \frac{1}{D(k)} \int_0^{\xi} \text{Ai}(\xi)d\xi, \quad \bar{V}_2 = -(ik)^{2/3} \int_0^{\xi} \bar{U}_2 d(\xi), \quad (A4)$$

where  $\xi = (ik)^{1/3}Y$  and  $D(k) = 1/3 - (ik)^{-1/3}k^{-1}\text{Ai}'(0)$ .

The excited perturbation in the spectrum space is governed by

$$\frac{d^3 \tilde{U}_2}{d\xi^3} - \xi \frac{d\tilde{U}_2}{d\xi} = Q \equiv (ik)^{-1} \frac{d}{dY} (ik\hat{U}_a \bar{U}_2 + \bar{V}_2 \hat{U}_{a,Y}); \quad (A5)$$

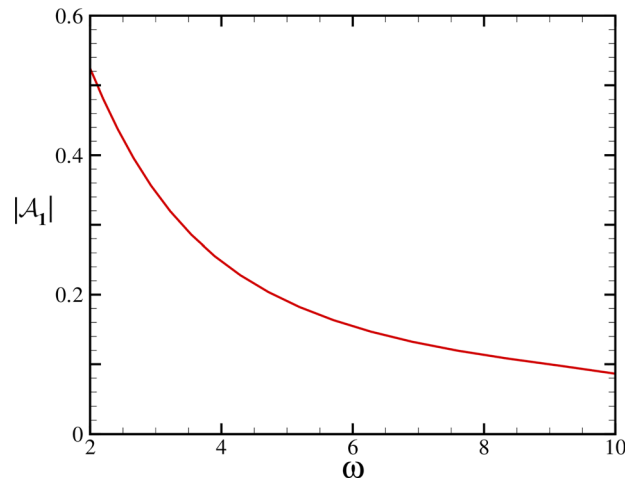


FIG. 11. Dependence of the linear receptivity efficiency  $\mathcal{A}_1$  on  $\omega$ .

$$\tilde{U}_2(k, \zeta_0) = 0, \quad (ik)^{1/3} \tilde{P}_2 = \frac{d^2 \tilde{U}_2(k, \zeta_0)}{d\zeta^2}, \quad \tilde{U}_2(k, \infty) \rightarrow \tilde{P}_2/k, \quad (A6)$$

where  $\zeta$  and  $\zeta_0$  have been defined in (24) with  $\alpha$  being replaced by  $k$ . Solving the above system, we obtain

$$\tilde{P}_2 = \frac{k \text{Ai}'(\zeta_0) \int_{\zeta_0}^{\infty} G(\zeta) d\zeta}{\text{Ai}'(\zeta_0) - (ik)^{1/3} k \int_{\zeta_0}^{\infty} \text{Ai}(\zeta) d\zeta}, \quad (A7)$$

where  $G(\zeta)$  is the solution of the boundary-value problem  $G'' - \zeta G = Q$ , with  $G'(\zeta_0) = 0$  and  $G(\infty) \rightarrow 0$ .

The pressure perturbation in the physical space is obtained by performing the inverse Fourier transform. Noting that the denominator is singular when the dispersion relation (25) is satisfied, then by closing the integral path in the upper-half complex plane, the inverse Fourier transform is estimated by use of the residual theorem,

$$\tilde{P} = U_s \hat{f}(\alpha) \tilde{P}_1 \sim U_s \alpha \mathcal{A}_1 e^{i\alpha X}, \quad (A8)$$

where

$$\mathcal{A}_1 = \frac{i\alpha^{-1} \text{Ai}'(\bar{\zeta}_0) \int_{\bar{\zeta}_0}^{\infty} G(\zeta) d\zeta}{-\frac{4}{3} (i\alpha)^{1/3} \int_{\bar{\zeta}_0}^{\infty} \text{Ai}(\zeta) d\zeta + \frac{2}{3} \frac{\bar{\zeta}_0}{\alpha} \text{Ai}(\bar{\zeta}_0) [-\bar{\zeta}_0 + i(i\alpha)^{4/3}]} \quad (A9)$$

with  $\bar{\zeta}_0 = -i\omega(i\alpha)^{-2/3}$ .

Actually, the linear receptivity is the same as the roughness-acoustic receptivity,<sup>3,4,29</sup> with the shape function of the roughness being replaced by the Heaviside step function. The dependence of  $\mathcal{A}_1$  on  $\omega$  is plotted in Fig. 11 in which the monotonic decrease trend is observed.

## REFERENCES

- S. Barbarino, O. Bilgen, R. Ajaj, M. I. Friswell, and D. J. Inman, "A review of morphing aircraft," *J. Intell. Mater. Syst. Struct.* **22**, 823–877 (2011).

- <sup>2</sup>L. Chu, Q. Li, F. Gu, X. Du, Y. He, and Y. Deng, "Design, modeling, and control of morphing aircraft: A review," *Chin. J. Aeronaut.* **35**, 220–246 (2021).
- <sup>3</sup>A. I. Ruban, "On Tollmien-Schlichting wave generation by sound (in Russian)," *Izv. Akad. Nauk SSSR Mekh. Zhidk. Gaza* **5**, 44–52 (1984), [*Fluid Dyn.* **19**, 709–717 (1984)].
- <sup>4</sup>M. E. Goldstein, "Scattering of acoustic waves into Tollmien-Schlichting waves by small streamwise variations in surface geometry," *J. Fluid Mech.* **154**, 509–530 (1985).
- <sup>5</sup>P. W. Duck, A. I. Ruban, and C. N. Zhikarev, "Generation of Tollmien-Schlichting waves by free-stream turbulence," *J. Fluid Mech.* **312**, 341–371 (1996).
- <sup>6</sup>X. Wu, "On local boundary-layer receptivity to vortical disturbances in the free stream," *J. Fluid Mech.* **449**, 373–393 (2001).
- <sup>7</sup>A. I. Ruban, S. K. Keshari, and M. A. Kravtsova, "On boundary-layer receptivity to entropy wave," *J. Fluid Mech.* **929**, A17 (2021).
- <sup>8</sup>X. Wu, "Generation of Tollmien-Schlichting waves by convecting gusts interacting with sound," *J. Fluid Mech.* **397**, 285–316 (1999).
- <sup>9</sup>A. I. Ruban, T. Bernots, and M. A. Kravtsova, "Linear and nonlinear receptivity of the boundary layer in transonic flows," *J. Fluid Mech.* **786**, 154–189 (2016).
- <sup>10</sup>Y. Liu, M. Dong, and X. Wu, "Generation of first Mack modes in supersonic boundary layers by slow acoustic waves interacting with streamwise isolated wall roughness," *J. Fluid Mech.* **888**, A10 (2020).
- <sup>11</sup>M. Dong, Y. Liu, and X. Wu, "Receptivity of inviscid modes in supersonic boundary layers due to scattering of freestream sound by wall roughness," *J. Fluid Mech.* **896**, A23 (2020).
- <sup>12</sup>X. Wu and M. Dong, "A local scattering theory for the effects of isolated roughness on boundary-layer instability and transition: Transmission coefficient as an eigenvalue," *J. Fluid Mech.* **794**, 68–108 (2016).
- <sup>13</sup>M. Dong and A. Zhang, "Scattering of Tollmien-Schlichting waves as they pass over forward-/backward-facing steps," *Appl. Math. Mech.* **39**, 1411–1424 (2018).
- <sup>14</sup>L. Zhao and M. Dong, "Effect of suction on laminar-flow control in subsonic boundary layers with forward-/backward-facing steps," *Phys. Fluids* **32**, 054108 (2020).
- <sup>15</sup>M. Dong, "Scattering of Tollmien-Schlichting waves by localized roughness in transonic boundary layers," *Appl. Math. Mech.* **41**, 1105–1124 (2020).
- <sup>16</sup>M. Dong and L. Zhao, "An asymptotic theory of the roughness impact on inviscid Mack modes in supersonic/hypersonic boundary layers," *J. Fluid Mech.* **913**, A22 (2021).
- <sup>17</sup>L. Zhao and M. Dong, "Effect of surface temperature strips on the evolution of supersonic and hypersonic Mack modes: Asymptotic theory and numerical results," *Phys. Rev. Fluids* **7**, 053901 (2022).
- <sup>18</sup>L. Zhao, M. Dong, and Y. Yang, "Harmonic linearized Navier-Stokes equation on describing the effect of surface roughness on hypersonic boundary-layer transition," *Phys. Fluids* **31**, 034108 (2019).
- <sup>19</sup>J. Sumariva, S. Hein, and E. Valero, "On the influence of two-dimensional hump roughness on laminar-turbulent transition," *Phys. Fluids* **32**, 034102 (2020).
- <sup>20</sup>M. Dong and C. Li, "Effect of two-dimensional short rectangular indentations on hypersonic boundary-layer transition," *AIAA J.* **59**, 2368–2381 (2021).
- <sup>21</sup>Q. Tang, Y. Zhu, X. Chen, and C. Lee, "Development of second-mode instability in a Mach 6 flat plate boundary layer with two-dimensional roughness," *Phys. Fluids* **27**, 064105 (2015).
- <sup>22</sup>S. Chen and C. Lee, "Effect of cavity on hypersonic flat-plate boundary layer instability," *Phys. Fluids* **33**, 084109 (2021).
- <sup>23</sup>X. Wu and M. Dong, "Entrainment of short-wavelength free-stream vortical disturbances in compressible and incompressible boundary layers," *J. Fluid Mech.* **797**, 683–782 (2016).
- <sup>24</sup>K. Stewartson, "On the flow near the trailing edge of a flat plate," *Mathematika* **16**, 106–121 (1969).
- <sup>25</sup>F. T. Smith, "Laminar flow over a small hump on flat plate," *J. Fluid Mech.* **57**, 803–824 (1973).
- <sup>26</sup>F. T. Smith, "On the non-parallel flow stability of the Blasius boundary layer," *Proc. R. Soc. Lond. A* **366**, 91–109 (1979).
- <sup>27</sup>M. Abramowitz and I. A. Stegun, *Handbook of Mathematical Functions with Formulas, Graphs and Mathematical Tables* (National Bureau of Standards, 1964).
- <sup>28</sup>M. Dong and X. Wu, "Generation of convective instability modes in the wake flow of the trailing edge of a flat plate," AIAA Paper No. AIAA 2017–4022, 2017.
- <sup>29</sup>N. De Tullio and A. I. Ruban, "A numerical evaluation of the asymptotic theory of receptivity for subsonic compressible boundary layers," *J. Fluid Mech.* **771**, 520–546 (2015).